Available online at www.sciencedirect.com
SCIENCE DIRECT
ELSEVIER
Solar Energy 74 (2003) 33–44
SOLAR ENERGY

Performance analysis of a solar-assisted heat pump water heater

J.P. Chyng, C.P. Lee, B.J. Huang*
Department of Mechanical Engineering, National Taiwan University, Taipei 106, Taiwan

Abstract

A modeling and system simulation of an integral-type solar assisted heat pump water heater (ISAHP) was carried out in the present study. The modeling and simulation assumes a quasi-steady process for all the components in the ISAHP except the storage tank. The simulation results for instantaneous performance agreed very well with experiment. The simulation technique was used to analyze the daily performance of an ISAHP for 1 year. It is shown that the daily total COP (COP_o) is around 1.7 to 2.5 year around for the ISAHP, depending on seasons and weather conditions. COP_o is higher than 2.0 for most of the time in a year and the daily operating time varies from 4 to 8 h. The online adjustment requirement of the expansion valve was also investigated using the present simulation technique. The analysis shows that the expansion device does not need to be controlled online. Using the 1-year simulation results, a universal daily performance correlation of the ISAHP was derived and shown experimentally to be applicable to another design of ISAHP.

1. Introduction

A direct expansion solar assisted heat pump (SAHP) water heater consists of a Rankine refrigeration cycle coupled with a solar collector that acts as an evaporator. The refrigerant is directly expanded inside the evaporator to absorb the solar energy. By a proper design of the Rankine refrigeration cycle and the collector for a specific operating condition, heat may be absorbed from, rather than rejected to, the ambient. That is, SAHP can absorb heat from solar radiation and ambient air simultaneously (Huang and Chyng, 2001). Huang and Chyng (1999) first proposed the design of an integral-type solar-assisted heat pump water heater (ISAHP) that integrates the heat pump, solar collector and water storage tank together to come up with a single unit that is easy to install (see Fig. 1). Huang and Chyng (2001) further studied experimentally the instantaneous performance characteristics of an ISAHP operating at a near saturated-vapour state at the inlet of the compressor. It was also observed in the experiment that the expansion valve needs online adjustment in order to keep the ISAHP operating at a near saturated-vapour state. This implies that an automatic control system of the expansion valve may be required for the ISAHP.

An ISAHP absorbs solar radiation and ambient heat simultaneously. The water in the tank is heated from cold to hot (about 60 °C) daily. This makes the Rankine refrigeration cycle operate in a time-variable state. In addition, the weather conditions may vary severely and randomly, minute by minute or day by day. The operation of an ISAHP is therefore non-steady state. The regulation of the expansion device in the ISAHP thus can be a problem. In the present study, we carried out a system analysis for an ISAHP to understand the performance of the ISAHP including the required regulation of the expansion device. Both instantaneous, daily and yearly performance characteristics are studied. The analytical results are then compared with experimental data. The present study focuses on the performance of an ISAHP designed and fabricated previously by Huang and Chyng (2001). The schematic diagram is shown in Fig. 2.

2. Prototype design of an ISAHP

The ISAHP prototype used a bare collector/evaporator. The collector is of tube-in-sheet type using copper tube (6 mm diameter) and copper sheet (0.4 mm thick). Copper tubes are soldered on the copper sheet. The collector surface is divided into four parts: one top surface (50 cm×74 cm), one front surface (50 cm×120 cm) and two side surfaces (60 cm×74 cm each), as shown in Fig. 3. The total surface area of the collector is 1.86 m^2. The collector surface is painted in black. Three refrigerant flow channels

*Corresponding author. Tel.: +886-2-2363-4790; fax: +886-2-2364-0549.
E-mail address: bjhuang@seed.net.tw (B.J. Huang).

0038-092X/03/$ – see front matter
doi:10.1016/S0038-092X(03)00110-5

Nomenclature

A_c	area of solar collector, m^2
B_0 and B_1	flow friction parameters in Eq. (2)
c	fitted constant,
$c_{p,w}$	specific heat of water, J kg^{-1} $°C^{-1}$
COP_o	daily total coefficient of performance (COP) the total energy absorbed by water/total electrical consumption
D	inner diameter of water tank, m
Gr	Grashof number
H	height of water tank, m
H_{th}	thermosyphon pressure head, m H_2O
H_t	daily total solar irradiation, J m^{-2} day^{-1}
h	enthalpy, J kg^{-1}
I	solar irradiation upon horizontal surface, W m^{-2}
L	length of thermosyphon heat exchanger, m
M_w	total mass of water in the storage tank, kg
$\dot{m}$	mass flow rate, kg s^{-1}
$\dot{m}_H$	water mass flow rate of the tank inlet, kg s^{-1}
$\dot{m}_L$	mass flow rate of hot water load from the tank, kg s^{-1}
$\dot{m}_R$	refrigerant mass flow rate of the tank inlet, kg s^{-1}
$\dot{m}_w$	water mass flow rate in the thermosyphon loop, kg s^{-1}
N	number of stratified layer
P	pressure, MPa
P_c	condensing pressure, MPa
P_e	evaporating pressure, MPa
P_1	compressor suction pressure, MPa
P_2	compressor discharge pressure, MPa
Pr	Prandtl number
Q_e	evaporation heat rate, W
Q_c	condenser heat rate, W
Q_w	daily total energy collection, J
Re	Reynolds number
R_F	flow resistance of expansion valve, MPa s kg^{-1}
R_{F0}	daily initial flow resistance, MPa s kg^{-1}
S_{RF}	rate of change of R_F, MPa s^2 kg^{-1}
t	time, s
T	temperature, °C
T_a	ambient air temperature, °C
$T_{a,av}$	mean ambient air temperature during operation of ISAHP, °C
T_c	condensing temperature, °C
T_e	evaporation temperature, °C
$T_{e,av}$	mean evaporation temperature during operation of ISAHP, °C
T_{hx}	water temperature in the thermosyphon heat exchanger, °C
$T_{hx,w}$	water temperature in the thermosyphon heat exchanger, °C
$T_{hx,in}$	water temperature at the inlet of the thermosyphon heat exchanger, °C
$T_{hx,out}$	water temperature at the outlet of the thermosyphon heat exchanger, °C
$T_{in,R}$	refrigerant temperature at the inlet of thermosyphon heat exchanger, °C
$T_{out,R}$	refrigerant temperature at the outlet of thermosyphon heat exchanger, °C
$T_{in,w}$	water temperature at the inlet of thermosyphon heat exchanger, °C
$T_{out,w}$	water temperature at the outlet of thermosyphon heat exchanger, °C
T_w	water temperature in the tank, °C
$T_{w,av}$	average water temperature in the tank, °C
T_{wi}	daily initial water temperature in the tank, °C
U_c	heat transfer coefficient between air and collector surface, W m^{-2} $°C^{-1}$
$(UA)_{hx}$	overall heat transfer coefficient in thermosyphon heat exchanger, W $°C^{-1}$
$(UA)_e$	daily overall heat transfer coefficient from ambient to collector, W $°C^{-1}$
V_{SD}	rate of stroke volume of compressor, m^3 s^{-1}
W_{comp}	compressor input energy, J
z	vertical distance, m
α	absorption coefficient of collector surface
α_s	daily total solar energy absorption coefficient, Eq. (22)
α_i, β_i, γ_i	Boolean function in Eq. (5)
γ_w	specific weight of water
υ_w	kinematic viscosity, m^2 s^{-1}
υ	specific volume at compressor suction port, m^3 kg^{-1}
η_v	volumetric efficiency

Subscript

a	air
av	average
c	condenser
e	evaporator
H	heating
hx	heat exchanger
i	ith segment of water in tank
in	inlet of heat exchanger
out	outlet of heat exchanger
R	refrigerant
w	water
1, 2, 3, 4	state

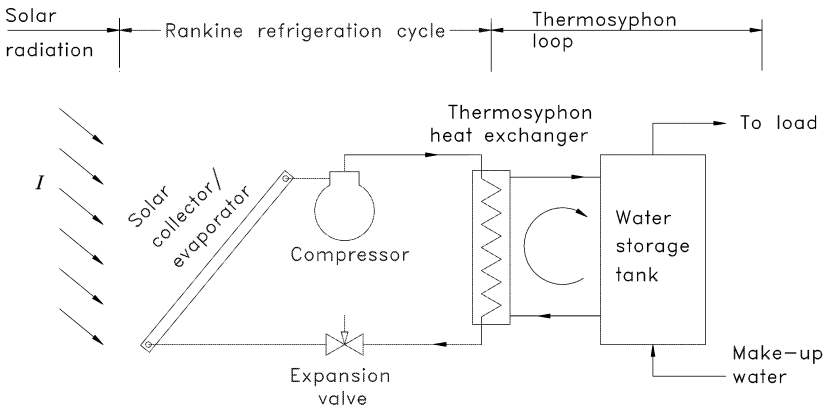

Fig. 1. Schematic diagram of the ISAHP.

are made along the directions of front-to-top and side-to-top, all connected in parallel (Fig. 3).

The Rankine refrigeration cycle unit is mounted inside the ISAHP. A small R134a reciprocating-type hermetic compressor with piston swept volume 5.29 cc, speed 3520 rev./min and rated input power 250 W is adopted.

The design of the thermosyphon heat exchanger in the thermosyphon loop is shown in Fig. 4. A helical coil made of copper tube with 6 mm diameter is immersed inside a straight water pipe. Water absorbs the condensation heat from the refrigerant vapor inside the copper tube and induces a buoyancy force for natural circulation along the loop. The ISAHP uses a 105-l tank for hot water storage.

An expansion valve (Model AEL-1, Egelhof, Germany) is used for regulating the refrigerant flow in the Rankine refrigeration cycle. A receiver and a filter are installed downstream from the condenser and an accumulator is installed downstream from the collector/evaporator to protect the compressor from wet compression.

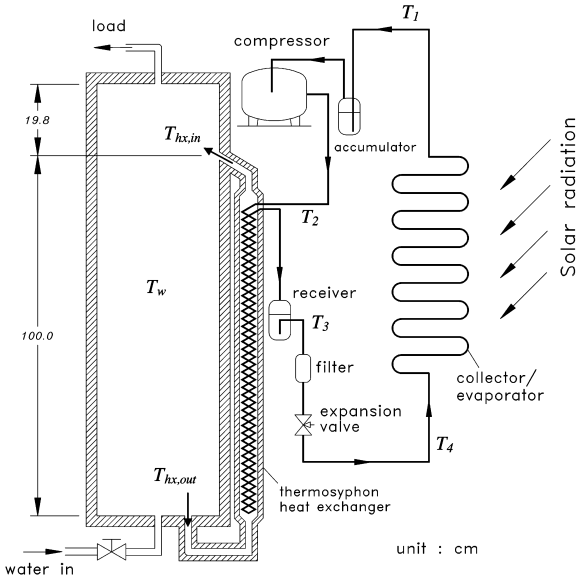

Fig. 2. Schematic diagram of the integral-type solar assisted heat pump.

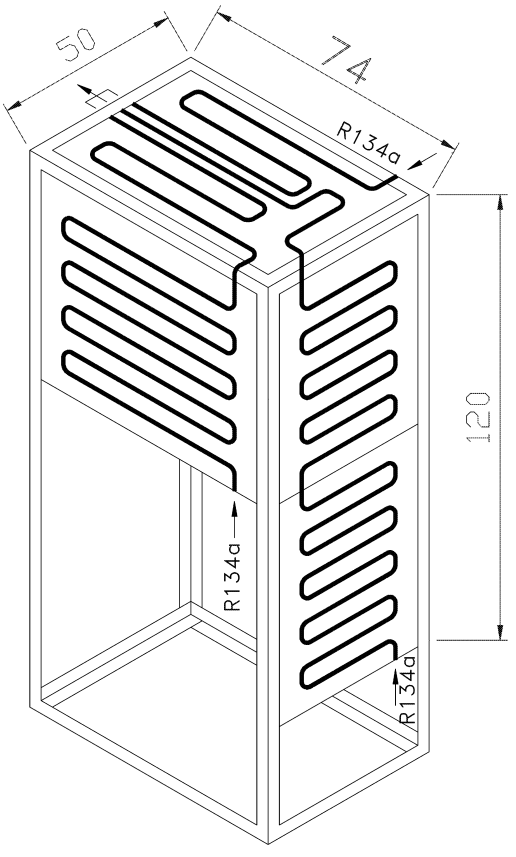

Fig. 3. Collector surface design of the ISAHP.

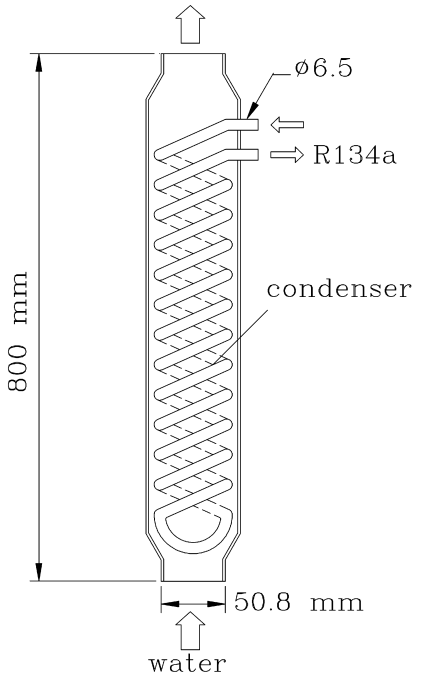

Fig. 4. Design of thermosyphon heat exchanger.

3. Mathematical model of the ISAHP

As seen from Fig. 1, the ISAHP absorbs energy from solar radiation and ambient air simultaneously using the principle of the Rankine refrigeration cycle. The solar collector/evaporator combines the evaporator of the Rankine cycle and the solar collector. A thermosyphon loop is used to transfer the heat from the condenser to the water tank via natural circulation. The thermosyphon heat exchanger combines the condenser of the Rankine cycle and the heater of the thermosyphon loop. The circulating flow-rate of the thermosyphon loop depends on the water temperature variations in the thermosyphon heat exchanger and in the water tank. The water temperature distribution in the thermosyphon heat exchanger is determined by the operation of the Rankine cycle that is affected by the design of the Rankine cycle machine and the variations of solar radiation and ambient conditions. Mathematical models of the components of ISAHP are derived first.

3.1. Momentum balance of the thermosyphon loop

The thermosyphon pressure head H_{th} induced in the thermosyphon loop can be evaluated by integrating the water density around the loop. The resulting equation is

$$H_{th} = \int_0^L [\gamma_w(T_w) - \gamma_w(T_{hx})]\,dz, \tag{1}$$

where γ_w is the specific weight of water that can be approximated by the relation:

$$\gamma_w(T) = -4.05\times10^{-6}T^2 - 3.906\times10^{-5}T + 1.0002556, \quad T \text{ in } ^\circ\text{C}. \tag{2}$$

The thermosyphon head H_{th} generated is used to overcome the flow resistance of the water circulation in the loop that is caused by pipe wall friction and other losses due to valves, bends and fittings, etc. in the loop. It can be assumed that the following quadratic function can be used to describe the loop flow resistance (Huang and Hsieh, 1985):

$$H_f = B_0 \nu_w \dot{m}_w + B_1 \dot{m}_w^2 \tag{3}$$

where ν_w is the kinematic viscosity of water and B_0 and B_1 are the coefficients that can be experimentally determined on site by measuring the mass flow-rate and pressure drop of the loop.

Since the variation of the flow-rate of the thermosyphon loop is slow, quasi-steady state can be assumed. Combining Eqs. (1) and (3), the governing equation for the momentum balance equation is,

$$\int_0^L [\gamma_w(T_w) - \gamma_w(T_{hx})]\,dz = B_0 \nu_w \dot{m}_w + B_1 \dot{m}_w^2. \tag{4}$$

Eq. (4) shows that the water flow-rate of the thermosyphon loop is affected by the water temperature distribution in the tank and the thermosyphon heat exchanger and the loop friction. For solving the flow rate, it is necessary to determine the temperature distributions first.

3.2. Water temperature distribution in storage tank

The thermal-stratification tank model developed by Close (1964) was verified experimentally (Huang et al., 1984) and has been successfully used in solar collector analysis (Huang and Hsieh, 1985). Close's model is thus used in the present study to calculate the water temperature distribution in the tank. The tank is divided into N well-mixed sections with convection and conduction with adjacent sections. The model assumes that the inlet hot water will flow to a section at the same temperature. An energy balance equation is derived for the ith segment of water (Close, 1964):

$$\frac{M_w c_{p,w}}{N}\frac{dT_i}{dt} = \underbrace{\frac{U_t \pi D H}{N}(T_a - T_i)}_{\text{Heat loss}} + \underbrace{\alpha_i \dot{m}_H c_{p,w}(T_{0,w} - T_i)}_{\text{Heat in}} + \underbrace{\beta_i \dot{m}_L c_{p,w}(T_{L,w} - T_i)}_{\text{Heat out}} + \underbrace{\begin{cases} \gamma_i c_{p,w}(T_{i-1} - T_i) & \text{if } \gamma_i > 0 \\ \gamma_i c_{p,w}(T_i - T_{i+1}) & \text{if } \gamma_i < 0 \end{cases}}_{\text{Internal conduction}} \tag{5}$$

where α, β, γ are the Boolean function defined as follows:

$$\alpha_i = \begin{cases} 1 & \text{if } T_{i-1} > T_0 > T_i \\ 0 & \text{other} \end{cases} \quad (6)$$

$$\beta_i = \begin{cases} 1 & \text{if } T_i > T_L > T_{i+1} \\ 0 & \text{other} \end{cases} \quad (7)$$

$$\gamma_i = \dot{m}_H \sum_{j=1}^{i-1} \alpha_j - \dot{m}_L \sum_{j=i+1}^{N} \beta_j. \quad (8)$$

Eq. (5) can be solved by the 4th order Runge–Kutta method. Using the Simpson 1/8 method, integrating the temperature profile with respect to height, the thermosyphon pressure head in the water storage tank is determined.

3.3. Condenser heat rejection rate

Heat rejection from the refrigeration cycle to the water tank occurs via the thermosyphon loop. Dahl and Davidson (1997) have derived experimentally an overall heat transfer correlation for a water thermosyphon loop heat exchanger identical to the present design:

$$(UA)_{hx} = 0.12 Pr^{0.43} Re^{0.13} Gr^{0.30}, \quad \text{W/°C}. \quad (9)$$

Eq. (9) can be approximated as the overall heat transfer coefficient from the refrigerant side to the water in the thermosyphon heat exchanger since the water side heat transfer dominates the heat transfer process. *Pr*, *Re*, *Gr* numbers as well as water properties are evaluated at the average of the inlet temperatures $(T_{in,R} + T_{in,w})/2$ of the heat exchanger. The characteristic temperature difference in the definition of *Gr* is $T_{in,R} - T_{in,w}$.

For a well-insulated heat exchanger, the rejected heat from the Rankine cycle is completely taken away by the thermosyphon loop water. Therefore,

$$\dot{m}_w c_{p,w}(T_{out,w} - T_{in,w}) = (UA)_{hx} \times \text{LMTD} \quad (10)$$

where LMTD (log mean temperature difference) is defined as

$$\text{LMTD} = \frac{(T_{out,R} - T_{in,w}) - (T_{in,R} - T_{out,w})}{\ln[(T_{out,R} - T_{in,w})/(T_{in,R} - T_{out,w})]}. \quad (11)$$

3.4. Water temperature distribution in heat exchanger

Since the design of the thermosyphon heat exchanger in the present ISAHP is a counter-flow type, the temperature distribution along the flow direction in the waterside can be approximated by a log function and expressed as

$$T_{hx,w}(z) = \frac{T_{out,w} - T_{in,w}}{\ln(L+1)} \ln(z+1) + T_{in,w}. \quad (12)$$

3.5. Rankine cycle model

R134a is the working fluid in the Rankine cycle. The refrigerant mass flow rate can be evaluated from the volumetric efficiency of the compressor given by the compressor manufacturer:

$$\dot{m}_R = \frac{\eta_v \times V_{SD}}{v} \quad (13)$$

$$\eta_v = -0.0163 \times \left(\frac{P_2}{P_1}\right) + 0.6563. \quad (14)$$

The energy balance of the condenser yields the following equation, assuming no heat loss:

$$\dot{m}_R(h_2 - h_3) = (UA)_{hx} \times \text{LMTD}. \quad (15)$$

For an isenthalpic process in the expansion device, we obtain the following equation:

$$h_3 = h_4. \quad (16)$$

3.6. Solar collector model

The solar collector acts as the evaporator of the Rankine cycle and collector of solar radiation and ambient heat. The energy balance equation is

$$Q_e = \alpha I A_c - U_c A_c (T_e - T_a). \quad (17)$$

4. Simulation procedure of ISAHP

The simulation of ISAHP performance includes the performance computation of the Rankine cycle and thermosyphon loop. The Rankine cycle and the thermosyphon loop are coupled through the condenser heat transfer. The Rankine cycle is first computed using the given meteorological data I and T_a. An iteration process is required to determine the condenser temperature T_c. The computation starts from an initial guess for T_c, then compute the Rankine cycle to obtain Q_c, T_e, and Q_e. Q_c is then used to compute the water loop performance to determine the water temperature distribution in the thermosyphon heat exchanger.

Computation of the thermosyphon loop performance starts from an assumed initial water temperature in the tank and guessing a water outlet temperature at the thermosyphon heat exchanger $T_{w,out}$. The thermosyphon mass flow rate m_w is first computed from the momentum balance equation of the thermosyphon loop, using the known temperature distributions in the heat exchanger and the tank. A new water outlet temperature at the thermosyphon heat exchanger $T_{w,out}$ (denoted $T'_{w,out}$) can be determined using the mass flow-rate m_w and Q_c obtained from Rankine cycle computation and the energy balance relation:

$$Q_c = \dot{m}_w c_{p,w}(T_{w,out} - T_{w,in}). \quad (18)$$

Iteration will proceed if the new $T_{w,out}$ is not the same as old $T_{w,out}$ until convergence. After convergence of $T_{w,out}$, a new Q_c can be determined from Eq. (10). Another iteration in Rankine cycle calculation will proceed by changing T_c if the new Q_c is not identical with the old Q_c, until convergence.

By iteration, the principle of energy balance can be conserved for each time step. Repeating the computation again and again for new meteorological data will give the performance of the ISAHP.

5. Experimental verification of simulation

Experiments were carried out for the ISAHP built previously (Huang and Chyng, 2001) (Fig. 2). From Table 1, experimental results for the average water temperature in the tank, $T_{w,av}$, are seen to be very close to the simulation results although the refrigerant vapor temperature at the inlet and the exit of the compressor, T_1 and T_2, have a larger deviation between experiment and simulation (Fig. 5). This is due to the ignorance of the dynamic effect in the modeling. The inlet temperature T_2 responds to solar radiation variation faster since the thermal capacitance effect of the solar collector is small as compared with the thermal mass of the water storage tank (>100 kg). Fig. 5 shows that the solar irradiation is not steady during the experiment. This causes a larger deviation in the prediction of vapor temperature T_2 since quasi-steady models were used for all parts of the simulation except the storage tank.

Table 1 shows that the average water temperature prediction is acceptable, mostly within ±3 °C error. This results in an error <10% for the daily total energy collection prediction.

6. Performance of ISAHP under various climatic conditions

Using simulation, we can analyze the daily and long-term performance of the ISAHP under various climatic conditions. The present simulation uses 1-year meteorological data collected on site in the laboratory from August 15, 1998 to August 7, 1999. The data contain solar radiation intensity incident upon the horizontal surface I

Table 1
Comparison of experiments and simulation

Time	Average water temperature in tank $T_{w,av}$, °C					
	Experiment	Simulation	Simulation − experiment	COP	Total solar radiation (MJ/m^2 day)	Electricity consumption (kWh)
July 28, 1999						
11:04	32.4	31.1	−1.3			
11:40	38.3	35.8	−2.5			
12:14	42.4	40.0	−2.4			
13:11	49.1	46.5	−2.6			
13:49	53.1	50.6	−2.5			
14:34	57.4	55.0	−2.4	2.4	4.84	1.27
July 30, 1999						
11:01	28.4	27.4	−1.0			
11:13	30.2	28.7	−1.5			
12:20	40.2	37.4	−2.8			
14:55	60.8	55.1	−5.7	2.8	10.45	1.41
August 2, 1999						
10:16	33.7	32.3	−1.4			
11:09	41.2	39.0	−2.2			
11:53	46.9	44.4	−2.5			
13:01	54.9	51.9	−3.0	2.63	3.67	0.98
August 3, 1999						
10:57	30.7	29.5	−1.2			
11:23	34.5	32.9	−1.6			
12:40	44.7	43.0	−1.7			
13:43	52.5	49.5	−3.0			
14:41	57.6	54.5	−3.1			
15:05	59.0	56.5	−2.5	2.3	5.05	1.48

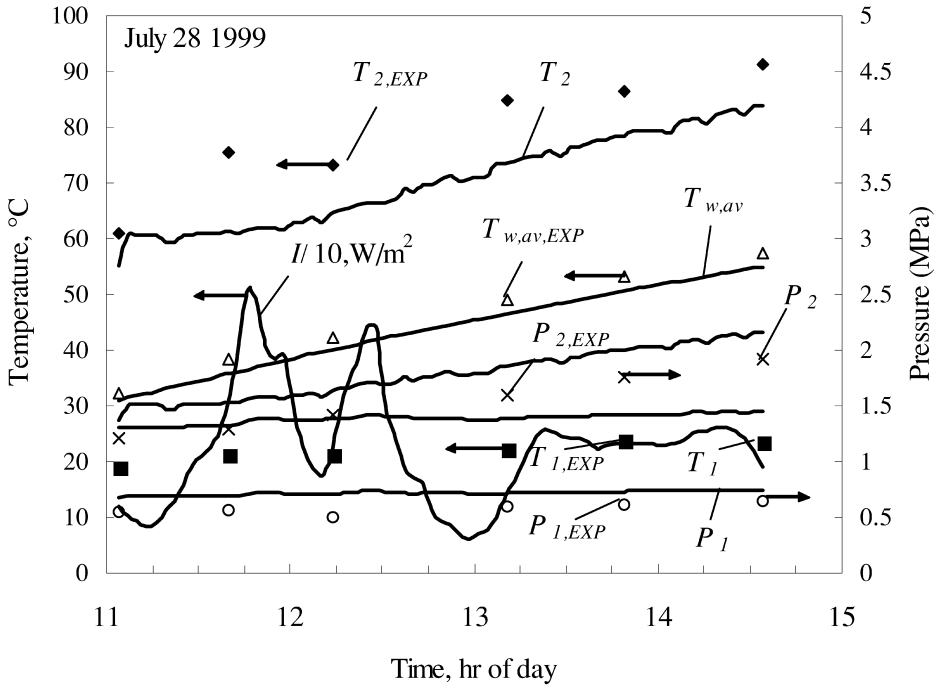

Tw : simulation water temperature.
Tw,exp: experimental water temperature.
T_1: simulation temperature at the inlet of the compressor.
T_1,EXP: experimental temperature at the inlet of the compressor.
T_2: simulation temperature at the outlet of the compressor.
T_2,EXP: experimental temperature at the outlet of the compressor.
P_1: simulation pressure at the inlet of the compressor.
$P_{1,exp}$: experimental pressure at the inlet of the compressor.
P_2: simulation pressure at the outlet of the compressor.
$P_{2,exp}$: experimental pressure at the outlet of the compressor.
I/10: solar radiation is divided by 10 ($W/m^2/10$)

Fig. 5. Comparison of experiment (symbols) and simulation (solid lines) for a single day.

and ambient temperature T_a, both were measured and averaged for every 3 min.

6.1. Daily performance analysis

The performance of ISAHP under various climatic conditions was studied. Four typical days representing four kinds of weather were selected for the study: namely, clear day ($15 < H_t < 20$ MJ/m^2 day, August 19, 1998); partly cloudy day ($10 < H_t < 15$ MJ/m^2 day, August 17, 1998); cloudy day ($5 < H_t < 10$ MJ/m^2 day, August 16, 1998); and rainy day ($0 < H_t < 5$ MJ/m^2 day, August 20, 1998).

Table 2
Performance of ISAHP at 09:00–15:00 h for various weather patterns

Weather pattern	H_t, MJ/m^2	COP_o (total)	W_{comp}, kJ	$T_{w,av}$, °C (final)
Clear day (August 19)	17.9	2.00	10 581	68.1
Partly cloudy (August 17)	12.8	2.00	10 099	66.1
Cloudy (August 16)	9.2	2.01	9724	64.5
Rainy (August 20)	3.2	2.03	8870	61.0

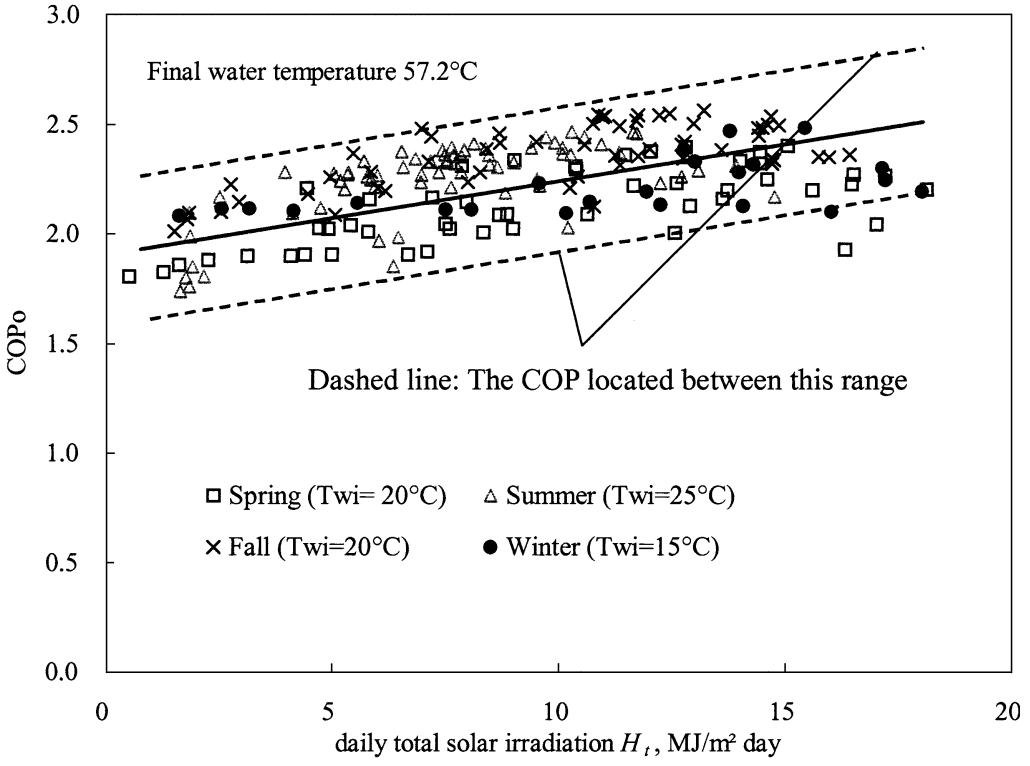

Fig. 6. Variation of daily total COP with solar irradiation.

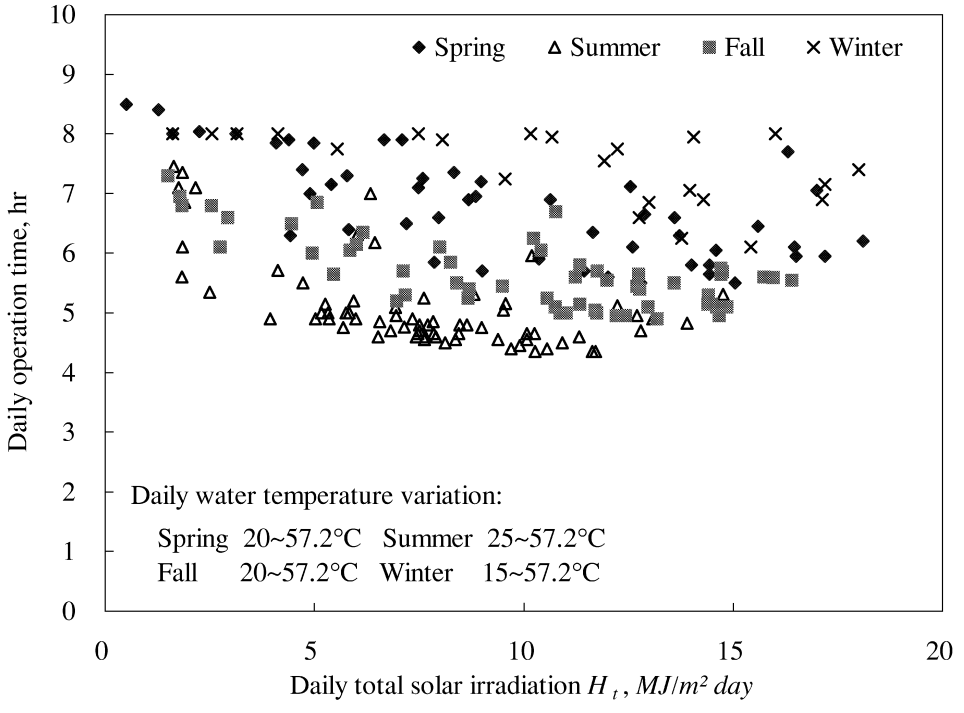

Fig. 7. Daily operation time of ISAHP.

The simulation results listed in Table 2 reveal that the final water temperature can reach 61 °C by 15:00 h on a rainy day. In this case, ISAHP absorbs energy mainly from ambient air (Huang and Chyng, 2001). Water temperature of 68 °C can be obtained by 15:00 h on a clear day. The total COPs are higher than 2.0.

The COP of the ISAHP can be increased if the final water temperature is set at a lower value. For domestic application, a final water temperature of 57.2 °C (135°F) is adopted in many places. The simulation was therefore repeated using the 1-year meteorological data and the results are shown in Fig. 6. COP_o in Fig. 6 represents the total COP of the ISAHP stopping operation whenever the average water temperature in the tank reaches 57.2 °C. The daily starting time is at 08:00 h in winter season, 08:30 h in spring and fall seasons, and 09:00 h in summer season. It is seen from Fig. 6 that, for different daily initial water temperatures, T_{wi}, in different seasons, COP_o increases with increasing daily solar irradiation H_t. COP_o is between 1.7 and 2.5 throughout the year. In general, COP_o is higher in summer and fall seasons. Since the COP of a heat pump water heater increases with decreasing initial water temperature and increasing ambient temperature (Huang and Lin, 1997), the COP_o of an ISAHP in summer may not be the highest, as indicated in Fig. 6. Fig. 6 shows that COP_o of an ISAHP is higher than 2.0 for most of the time in a year. The daily operation time of the ISAHP is shown in Fig. 7. The ISAHP operates longer in winter, 6 to 8 h, depending on daily total solar irradiation and ambient temperature. In summer, the ISAHP will operate between 4 and 7 h daily, with run times of around 4 to 5 h being typical.

6.2. Study of expansion valve adjustment for better performance

It has been shown in an experimental study (Huang and Chyng, 2001) that an ISAHP will operate at a high efficiency if the expansion valve is adjusted online to keep the refrigerant vapor at the inlet of the compressor close to

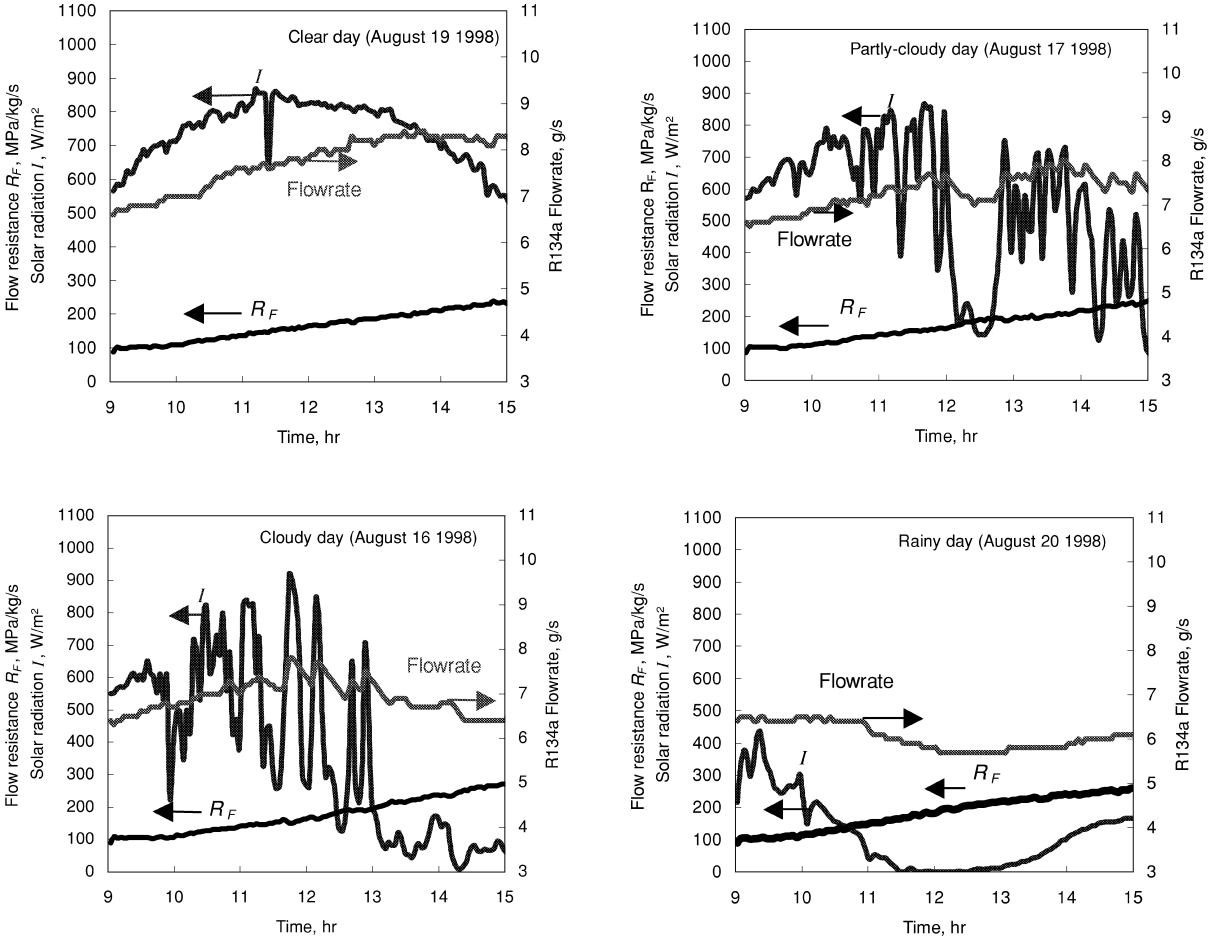

Fig. 8. Variation of refrigerant flow-rate and expansion valve resistance.

Table 3
Rate of change of expansion valve resistance for different climate patterns

Climate pattern	Clear day August 19	Partly-cloudy August 17	Cloudy August 16	Rainy August 20
Initial resistance R_{Fo}, MPa kg^{-1} s	78.8	73.4	72.6	85.2
Final resistance R_{Ft}, MPa kg^{-1} s	225.9	240.7	248.5	247.0
Variation of R_F in a day, folds	2.87	3.28	3.42	2.90
S_{RF}, MPa kg^{-1} s h^{-1}	24.5	27.9	29.3	27.0

a saturated-vapor state. The simulation tool developed in the present study can be used to study the online adjustment of the expansion valve under various climatic conditions. The adjustment of the expansion valve opening can be described using the flow resistance R_F:

$$R_F = (P_c - P_e)/\dot{m}_R. \quad (19)$$

Fig. 8 shows that R_F varies almost linearly with time during a day, irrespective of climatic conditions. This is caused by the large thermal masses of the solar collector and water that damp out the effect of solar radiation variation. The present result indicates that the expansion valve should be regulated gradually and approximately linearly during a day in order to keep the Rankine cycle at a saturated-vapor cycle. We can thus describe the instantaneous variation of R_F in the following relation:

$$R_F(t) = R_{Fo} + S_{RF}t \quad (20)$$

where S_{RF} is the rate of change of R_F. Table 3 shows that S_{RF} is small and approximately a constant irrelevant of the climate pattern. One-year simulation results also show that S_{RF} is small and approximates a constant as shown in Fig. 9. Figs. 8 and 9 indicate that the ISAHP need not be controlled online as long as the expansion device is properly designed with a mean resistance value.

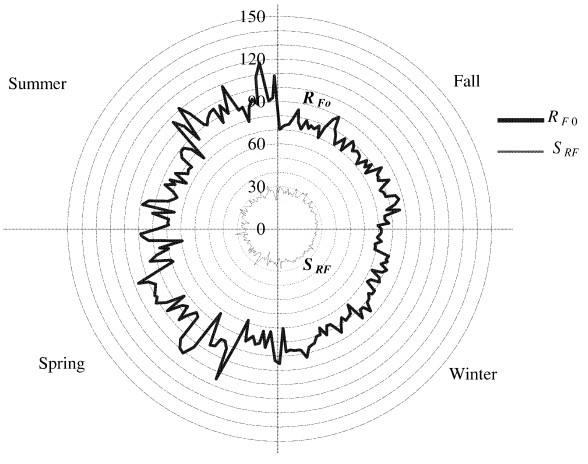

Fig. 9. Seasonal variation of S_{RF}.

6.3. Study of performance correlation of ISAHP

The simulation technique developed in the present study can be used to derive a correlation for the daily performance of ISAHP. The thermodynamic states at various locations of the Rankine cycle and the temperature variations in the water loop can be calculated using the simulation program and the meteorological data. A daily performance including total heat collection and thermal efficiency can be evaluated. Huang and Chyng (2001) have derived an instantaneous correlation of ISAHP for the total energy absorption at the evaporator:

$$\frac{Q_e}{I} = 50.1\frac{T_a - T_e}{I} + 0.844. \quad (21)$$

Eq. (21) implies that the following correlation may exist for daily performance data:

$$\frac{Q_w}{H_t} = (UA)_e\frac{T_{a,av} - T_{e,av}}{H_t} + \alpha_s \quad (22)$$

where Q_w is the daily total energy collection in the tank; $(UA)_e$ is the daily-total heat transfer coefficient from ambient air to the refrigerant inside the solar collector; α_s is the solar absorption coefficient representing energy collection from solar radiation.

Using 1-year meteorological data, a daily performance simulation was performed and the following correlation was obtained:

$$\frac{Q_w}{H_t} = 3.33\frac{T_{a,av} - T_{e,av}}{H_t} + 0.47. \quad (23)$$

The correlation is satisfactory as shown in Fig. 10. To check the applicability of the correlation (22) to other ISAHPs, an experiment was performed using another ISAHP (ISAHP-B). The design of ISAHP-B is basically the same as ISAHP but larger in size. The specifications are listed in Table 4. The experimental data are seen to fit the above correlation very well but with different parameters, as shown in Fig. 11:

$$\frac{Q_w}{H_t} = 2.36\frac{T_{a,av} - T_{e,av}}{H_t} + 0.53. \quad (24)$$

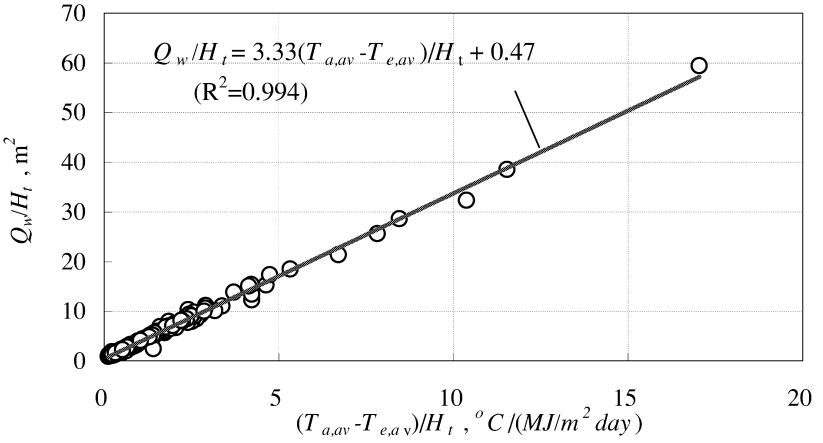

Fig. 10. Correlation of daily performance of ISAHP (simulation data).

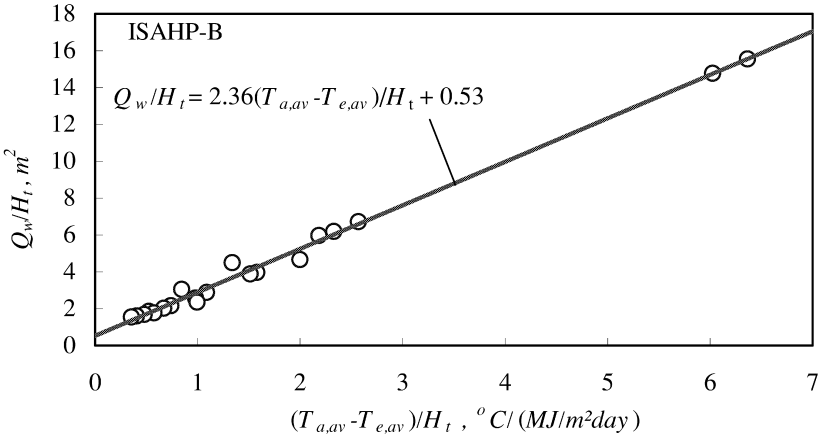

Fig. 11. Experimental correlation of daily performance of ISAHP-B (experimental data).

7. Discussion and conclusion

A modeling and system simulation of ISAHP for thermal performance analysis was carried out in the present study. The modeling and simulation assumes quasi-steady operation for all the components in the ISAHP except the storage tank. The simulation results for instantaneous performance agreed very well with experimental data. The simulation technique is then used to analyze the daily performance of ISAHP for 1 year. It is shown that the daily total COP (COP_o) is around 1.7 to 2.5 year round for the ISAHP, depending on season and

Table 4
Design specifications of ISAHP-B

Collector area	3.78 m^2 selective surface, unglazed
Water tank	240 l (50 cm diameter, 120 cm tall) 6 cm PU insulation layer
Rankine cycle:	Compressor/R134a, 600 W/110 VAC, 6 cm^3 Condenser/tube bundles (15 tubes, 12.7 mm I.D., 1 m long)

weather conditions. COP_o of the ISAHP is higher than 2.0 for most of the time in a year and the daily operating time varies in the range 4 to 8 h. For fixed final water temperature at 57.2 °C, the ISAHP operates longer in winter (6 to 8 h) and shorter in summer (4 to 7 h). This indicates that the Rankine cycle in the ISAHP is slightly oversized. The water storage capacity can be increased (to 120–150 l) in order to make better use of the heat pump.

It is better to keep ISAHP operating at a nearly saturated-vapor cycle in order to obtain a better efficiency. The online adjustment requirement of the expansion valve was investigated using the present simulation technique. The 1-year simulation result shows that the rate of valve opening regulation (S_{RF}) is small and approximates a constant. This indicates that ISAHP needs not to be controlled online as long as the expansion device is properly designed with a mean resistance value. This coincides with the field test result of the prototype ISAHP. That used a capillary tube as the fixed expansion device. The long-term performance of the ISAHP with a properly-designed capillary tube has shown satisfactory results.

Using the 1-year simulation results, a daily performance correlation of ISAHP was derived. The correlation, Eq. (22), is further experimentally shown to be applicable to another ISAHP. The system simulation technique developed in the present study provides a powerful tool for the design of ISAHP.

Acknowledgements

The present study was supported by the Energy Commission, Ministry of Economic Affairs, Taiwan.

References

Close, D.J., 1964. The performance of solar water heaters with natural circulations. Solar Energy 6, 33–40.

Dahl, S.D., Davidson, J.H., 1997. Performance and modeling of thermosyphon heat exchangers for solar water heaters. ASME J. Solar Energy Eng. 119, 193–200.

Huang, B.J., Hsieh, C.T., 1985. A simulation method for solar thermosyphon collector. Solar Energy 35 (1), 31–43.

Huang, B.J., Lin, F.H., 1997. A compact and fast temperature response heat pump water heater. In: ASME ASIA '97 Congress & Exhibition, Singapore, September 30–October 2, Paper no. 97-AA-26.

Huang, B.J., Chyng, J.P., 1999. Integral type solar-assisted heat pump water heater. Renew. Energy 16, 731–734.

Huang, B.J., Chyng, J.P., 2001. Performance characteristics of integral type solar-assisted heat pump. Solar Energy 71 (6), 403–414.

Huang, B.J., Tsuei, Y.M., Wu, H., 1984. Study of heat transfer in thermally stratified tanks. Proc. Natl. Sci. Council Republic China Phys. Sci. Eng. 8 (4), 267–276.